# ANALYSIS OF BREE'S CYLINDER WITH NONLINEAR KINEMATIC HARDENING BEHAVIOR[*]

## A. NAYEBI

Mechanical Engineering School, Shiraz University, Shiraz, I. R. of Iran
Email: nayebi@shirazu.ac.ir

**Abstract–** Bree's cylinder was used to show different material behaviors under constant mechanical and cyclic thermal gradient loadings. Bree showed different behaviors with the help of a diagram known by his name as Bree's diagram. In this research, the problem was reconsidered without his simplified hypothesis. The used material model is nonlinear kinematic hardening. The two dimensional problem and the Poisson's effect were considered. In order to obtain the Bree's diagram, return mapping algorithm was used. The results showed that the one dimensional model of Bree is conservative and the bi-dimensional Bree's diagram does not correspond to the complete model.

**Keywords–** Bree's diagram, cyclic loading, nonlinear kinematic hardening, primary and secondary stresses

## 1. INTRODUCTION

Cyclic loading is an important subject in the design of many mechanical elements. The behavior of these elements under different loadings depends on many factors; such as type of loading, material behavior and structure under loading and it can be elastic, elastic shakedown, plastic shakedown or ratcheting.

Thermal ratcheting is very important in the design of pressure vessels for fast breeder nuclear reactors. Bree [1, 2] showed the response of a thin cylindrical vessel under different constant mechanical and cyclic thermal loadings in a diagram known as Bree's diagram. A steady-state pressure load and a cyclic linear through-the-wall temperature distribution were applied. In his first analysis [1], Bree considered a one dimensional model, ignored the axial stress and used a perfect plastic material model. Although the effect of axial stress was studied in the second article [2], the coupling effects between axial and hoop stresses (Poisson's coefficient) were neglected. Ng and Nadarajah [3, 4] modeled the same problem by finite element method. They showed the ratchetting rate in the hoop direction, obtained by both models of Bree, is conservative, but the axial ratchetting rate predicted by the biaxial model is not.

Limited experimental tests have been done to verify the theoretical results. Because of the experimental difficulties, applying a cyclic thermal loading of a thin strip under a bending load is usually considered [5-8]. Therefore the classical Bree problem is studied by means of the pulley test in which a wire or strip specimen is subjected to combined steady tensile stress combined with a cyclic bending stress. Brockfield and Moreton [8] showed that the limits obtained in the one dimensional Bree's diagram, which is a part of ASME design code [9], is conservative. This is due to the fact that Bree used the perfect plastic material model which enabled him to get an analytical solution for the problem. The real material behavior is usually more complicated. Govindararajan and Sundararajan [10] modified the Bree's analysis by considering Prager's linear kinematic hardening model using a successive numerical method. However, their analysis was limited to the first part of the Bree's diagram.

Later, Mahbadi and Eslami [11] showed that Prager's model cannot correctly simulate the material behavior. They analyzed a thick pressure vessel under cyclic thermal and mechanical loading, assuming that the material would behave according to the nonlinear kinematic hardening model of Armstrong and Frederick [12]. But they did not discuss all parts of Bree's diagram, which is important in the design of pressure vessels. Although many kinematic hardening models were proposed which describe some of the material behaviors in cyclic loadings [13], the Armstrong-Frederick model is less complex than the new models and gives a proper description of the essential material behavior.

In this paper, we use the Armstrong-Frederick model to study the response of a thin cylindrical shell under constant mechanical loading and a cyclic thermal gradient across the shell wall. The use of the return mapping algorithm permits us to determine the structure behavior under different combinations of loadings.

## 2. CLOSED – TUBE BIAXIAL-STRESS MODEL

We consider a thin-wall cylinder with a mean radius *R* and a wall thickness *t* (Fig. 1). The cylinder is closed at both ends and subjected to an internal pressure p and a heat flux through its internal surface. It is assumed that the temperature decreases from the inner surface of the cylinder to the outer surface and the temperature difference varies between ΔT and zero. We assume that the cylindrical shell is very long so the end effects and the curvature can be neglected.

The axial strain $\varepsilon_z$ and the hoop strain $\varepsilon_\theta$, are independent of the coordinates because of the bending prevention, but the strains change in each cycle. The axial stress $\sigma_z$ and the hoop stress $\sigma_\theta$, vary along the thickness and are only dependent on the coordinate x which is taken to be zero at the middle of the thickness of the cylinder as shown in Fig. 1. Using the equilibrium conditions, we have:

$$\int_{\frac{-t}{2}}^{\frac{t}{2}} \sigma_\theta dx = pR \tag{1}$$

$$\int_{\frac{-t}{2}}^{\frac{t}{2}} \sigma_z dx = \frac{pR}{2} \tag{2}$$
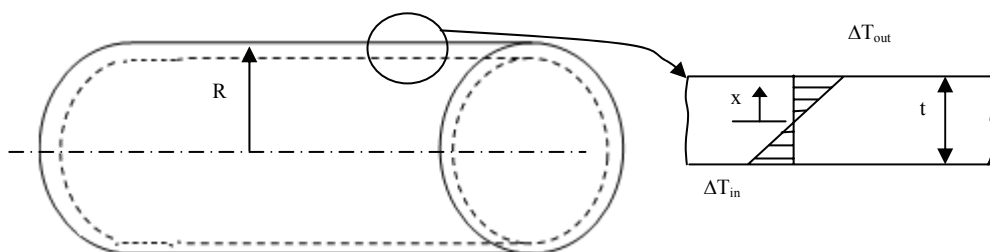


Fig. 1. Schematic representation of the closed tube and the temperature
gradient across the tube thickness

So every element of the tube is subjected to the mean stress $\frac{pR}{2t}$ in the axial and $\frac{pR}{t}$ in the hoop direction. The temperature gradient in the start up half cycle was supposed to vary linearly with respect to x. It is zero in the can mid-wall and during the shutdown second half cycle:

$$\Delta T_x = -\frac{x}{t} \Delta T \tag{3}$$

where $\Delta T$ is the temperature difference between the interior and the outer surface of the tube. The mean temperature in each cycle is considered sufficiently low so that the creep effects are negligible. The loading steps are demonstrated in Fig. 2.

Since bending is prevented, $\varepsilon_\theta$ and $\varepsilon_z$ are constants across the tube thickness. Therefore, the mean strain in both directions and for every loading is constant:
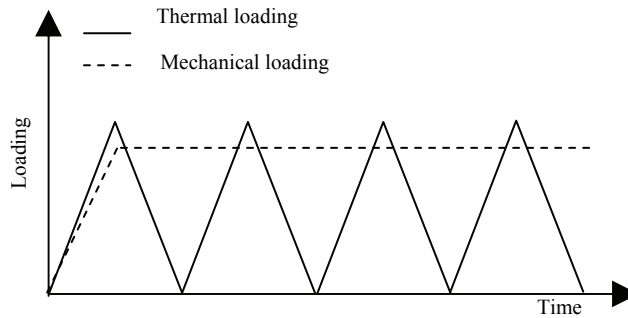


Fig. 2. Cyclic mechanical and thermal loading pattern

$$\int_{\frac{-t}{2}}^{\frac{t}{2}} \varepsilon_\theta dx = K_1 \tag{4}$$

$$\int_{\frac{-t}{2}}^{\frac{t}{2}} \varepsilon_z dx = K_2 \tag{5}$$

According to the strain partition principle, the strains in the hoop and axial directions can be decomposed into three parts (in small strain hypothesis): elastic, thermal and plastic strains. The total strains in the hoop and axial directions are given by:

$$\varepsilon_\theta = \varepsilon_\theta^e + \varepsilon_\theta^T + \varepsilon_\theta^p = \left( \frac{\sigma_\theta}{E} - \upsilon \frac{\sigma_z}{E} \right) + \alpha \Delta T_x + \varepsilon_\theta^p \tag{6}$$

$$\varepsilon_z = \varepsilon_z^e + \varepsilon_z^T + \varepsilon_z^p = \left( \frac{\sigma_z}{E} - \upsilon \frac{\sigma_\theta}{E} \right) + \alpha \Delta T_x + \varepsilon_z^p \tag{7}$$

where $\varepsilon^e$, $\varepsilon^T$ and $\varepsilon^p$ are, respectively, elastic, thermal and plastic strains. Equations (4-7) can be used to obtain hoop and axial stresses as:

$$\sigma_\theta = \frac{E}{1-\upsilon^2} \left( K_1 + \upsilon K_2 - (1+\upsilon)\alpha \Delta T_x - \varepsilon_\theta^p - \upsilon \varepsilon_z^p \right) \tag{8}$$

$$\sigma_z = \frac{E}{1-\upsilon^2} \left( K_2 + \upsilon K_1 - (1+\upsilon)\alpha \Delta T_x - \varepsilon_z^p - \upsilon \varepsilon_\theta^p \right) \tag{9}$$

Equations (6) and (7) can be substituted into Eqs. (4) and (5) to obtain the mean axial and hoop strains. Using Eqs. (1) and (2), we can obtain the constants $K_1$ and $K_2$ as:

$$K_1 = \left( 1 - \frac{\upsilon}{2} \right) \frac{pr}{Et} + \frac{1}{t} \int_{\frac{-t}{2}}^{\frac{t}{2}} \varepsilon_\theta^p dx \tag{10}$$

$$K_2 = \left(\frac{1}{2} - \upsilon\right)\frac{pr}{Et} + \frac{1}{t}\int_{\frac{-t}{2}}^{\frac{t}{2}}\varepsilon_z^p dx \tag{11}$$

Substituting the relations of $K_1$ and $K_2$ from Eqs. (10) and (11) into Eqs. (8) and (9), and noting that $\sigma_p = \dfrac{PR}{t}$ and $\sigma_{th} = \dfrac{E\alpha\Delta T}{2(1-\upsilon)}$ as it was considered by Bree, the axial and hoop stresses can be obtained as a function of plastic strains as:

$$\sigma_\theta = \sigma_p + \sigma_{th}\left(\frac{2x}{t}\right) + \frac{E}{\left(1-\upsilon^2\right)}\left[\frac{1}{t}\int_{\frac{-t}{2}}^{\frac{t}{2}}\left(\varepsilon_\theta^p + \upsilon\varepsilon_z^p\right)dx - \left(\varepsilon_\theta^p + \upsilon\varepsilon_z^p\right)\right] \tag{12}$$

$$\sigma_z = \frac{\sigma_p}{2} + \sigma_{th}\left(\frac{2x}{t}\right) + \frac{E}{\left(1-\upsilon^2\right)}\left[\frac{1}{t}\int_{\frac{-t}{2}}^{\frac{t}{2}}\left(\varepsilon_z^p + \upsilon\varepsilon_\theta^p\right)dx - \left(\varepsilon_z^p + \upsilon\varepsilon_\theta^p\right)\right] \tag{13}$$

Plastic strains can be determined from the constitutive relations including: the yield criteria, the normality rule and the back stress model. These relations are developed in the next section.

## 3. PLASTIC FLOW CONSTITUTIVE RELATIONS

In this study, we consider nonlinear kinematic hardening and use the concept of the yield surface, which obeys the Von-Mises yield criterion:

$$f = J_2(\boldsymbol{\sigma} - \mathbf{x}) - \sigma_y = 0 \tag{14}$$

$$J_2(\boldsymbol{\sigma} - \mathbf{x}) = \left[\frac{3}{2}(\boldsymbol{\sigma}' - \mathbf{x}') : (\boldsymbol{\sigma}' - \mathbf{x}')\right]^{\frac{1}{2}} \tag{15}$$

where x' is the deviatoric back stress which defines the position of the yield surface and $\sigma_y$ is the yield surface size. The plastic flow follows the normality rule:

$$d\boldsymbol{\varepsilon}^p = d\lambda\frac{\partial f}{\partial\boldsymbol{\sigma}} = \frac{3}{2}d\lambda\frac{\boldsymbol{\sigma}' - \mathbf{x}'}{\sigma_y} \tag{16}$$

The plastic multiplier $d\lambda$ can be derived from the consistency condition, $f = df = 0$, if plastic flow occurs. The usual linear-kinematic rule can be easily modified in order to introduce some non linear evolution, with an acceptable description of cyclic loadings (concavity of the stress-strain curves under tensile-compressive loading, for example). This modification, initially proposed by Armstrong and Frederick [12], in which an evanescent strain memory effect is introduced (evanescent along the plastic strain path), can be written in its simplest form as [14-15] as:

$$d\mathbf{x} = 2/3Cd\boldsymbol{\varepsilon}^p + \gamma\mathbf{d}\zeta \tag{17}$$

where C and $\gamma$ are the materials positive constant values. The accumulated plastic strain increment is

$$d\zeta = (2/3d\boldsymbol{\varepsilon}^p : d\boldsymbol{\varepsilon}^p)^{1/2} \tag{18}$$

The yield criteria for the biaxial stress can be obtained from the von-Mises yield criteria as:

$$f = (\sigma_\theta - x_\theta)^2 + (\sigma_z - x_z)^2 - (\sigma_\theta - x_\theta)(\sigma_z - x_z) - \sigma_y^2 = 0 \tag{19}$$

Using the normality rule, Eq. (16), we can express the relation between the hoop and the axial plastic strain increment as:

$$\frac{d\varepsilon_z^p}{d\varepsilon_\theta^p} = \frac{2\sigma_z - \sigma_\theta - 2x_z + x_\theta}{2\sigma_\theta - \sigma_z - 2x_\theta + x_z} \tag{20}$$

We solve Eqs. (12), (13), (19) and (20) together in order to obtain the response of the the closed-tube.

## 4. NUMERICAL SOLUTION

Because of the incremental nature of the developed relations, a numerical solution is required [16]. In this research the return mapping algorithm (RMA) was used. RMA [17, 18] represent a well established integration scheme to integrate the rate constitutive equations. This method consists of an elastic trial and a plastic corrector step. When the yield function is convex, that is, $f_n^{trial} > f_n$ at time step n, the elastic trial step is employed to characterize the plastic loading/unloading state of the material by using the algorithmic Kuhn-Tucker conditions:

$$f_n \leq 0, \ \Delta\lambda_n \leq 0, \ \Delta\lambda_n f_n = 0 \tag{21}$$

At each time step, the yield function is evaluated at the trial elastic step, in order to determine whether or not the plastic flow occurs. If the trial yield function is less than zero, then the material is assumed to be under elastic loading or elastic unloading. Otherwise, the material is subjected to the plastic loading. The normality rule is used to define the plastic strain increment in the radial RMA. According to the normality rule, the plastic strain increment is assumed to be in the direction of the normal of the yield surface, which is defined in the deviatoric stress space. The magnitude of the plastic strain increment is uniquely defined by the plastic multiplier. In order to determine the incremental value of the plastic multiplier $\Delta\gamma_n$ at the current time step *n*, the equation that ensures that the yield function is equal to zero is solved to determine $\Delta\gamma_n$. Since a nonlinear kinematic hardening model is assumed, then an iterative procedure such as the Newton-Raphson method is used to determine the plastic strain at the current time step. The plastic strains, the hardening parameter and the stress tensor are updated at the current time step by the determination of $\Delta\gamma_n$ (Fig. 3).

### *a) RMA formulation*

With the help of the deviatoric stress definition ($\boldsymbol{\sigma}' = P\boldsymbol{\sigma}$) and effective stress as $\boldsymbol{\tau} = \boldsymbol{\sigma} - \mathbf{x}$, the Von-Mises yield function becomes:

$$F = 1/2\boldsymbol{\tau}^T P\boldsymbol{\tau} - 1/3\sigma_y^2 \leq 0 \tag{22}$$

Using the normality rule, the increment of plastic strain can be obtained as

$$d\boldsymbol{\varepsilon}^p = d\lambda\frac{\partial F}{\partial\boldsymbol{\sigma}} = d\lambda P\boldsymbol{\tau} \tag{23}$$

So the plastic strain increment can be replaced in the accumulated plastic strain increment definition:

$$d\varsigma = \frac{2}{3}d\lambda\sigma_y \tag{24}$$

and the Armstrong-Fredrick nonlinear kinematic hardening reduces to:

$$d\mathbf{x} = \frac{2}{3}C\left(QP\boldsymbol{\tau} - \sigma_y\mathbf{x}\right)d\lambda \tag{25}$$

Using the Euler implicit method, the incremental form of relations (22-25), stress-strain and back stress equations can be written as:

$$\tau_{n+1} = \sigma_{n+1} - X_{n+1} \tag{26}$$

$$f_{n+1} = \frac{1}{2}\tau_{n+1}^T P\tau_{n+1} - \frac{1}{3}\sigma_y^2 \le 0 \tag{27}$$

$$\varepsilon_{n+1}^p = \varepsilon_n^p + P\tau_{n+1}\Delta\lambda_{n+1} \tag{28}$$

$$\varsigma_{n+1} = \varsigma_n + \frac{2}{3}\sigma_y\Delta\lambda_{n+1} \tag{29}$$

$$\sigma_{n+1} = C\left(\varepsilon_{n+1} - \varepsilon_n^p\right) - CP\tau_{n+1}\Delta\lambda_{n+1}. \tag{30}$$

$$\mathbf{x}_{n+1} = A^{-1}\mathbf{x}_n + \Delta\lambda_{n+1}\frac{2}{3}CA^{-1}P\tau_{n+1} \tag{31}$$

$$\text{where } A = 1 + \frac{2}{3}C\sigma_y\Delta\lambda_{n+1} \tag{32}$$

Hopperstad and Remseth [19] proposed to rewrite the effective stress, $\tau$, in terms of its eigenvectors, $\upsilon_k$ and eigenvalues $\zeta_k$, as:

$$\tau_{n+1} = \sum_{k=1}^{3}\zeta_k\upsilon_k \tag{33}$$

By substituting Eqs. (30-33) in Eq. (26), the eigenvalues can be obtained as:

$$\zeta_k = \frac{\alpha_k}{1 + \Delta\lambda\left(\frac{2}{3}CQA^{-1} + \mu_k\right)} \tag{34}$$

where $\alpha_k = \upsilon_k^T C^{-1}\tau_{n+1}^{trial}$ and $\tau_{n+1}^{trial} = C(\varepsilon_{n+1} - \varepsilon_n^p) - A^{-1}\mathbf{x}_n$.

Substituting Eq. (34) into (33) and utilizing the results in the Eq. (27), one can write the yield function as:

$$f_{n+1} = \frac{1}{2}\sum_{k=1}^{3}\mu_k\frac{\alpha_k^2}{\left[1 + \Delta\lambda_{n+1}\left(\frac{2}{3}CQA^{-1} + \mu_k\right)\right]^2} - \frac{1}{3}\sigma_y^2 = 0 \tag{35}$$

In order to determine $\Delta\lambda_{n+1}$, the above equation can be solved by the Newton-Raphson method.

### b) Application to the Bree's problem

Since the radial stress was ignored, the plane stress can be considered. The stress tensor can be written as: $\sigma = \begin{bmatrix} \sigma_\theta & \sigma_z & 0 \end{bmatrix}$. In order to apply the RMA, the thermal gradient, $\Delta T$, was divided into m steps. It is supposed that the mechanical loading does not cause any plastic flow. Trial elastic solution in the (n+1) step, which is needed by RMA, can be obtained from Eqs. (12, 13) as:

$$\begin{cases} \sigma_{\theta,n+1}^{Trial} = \sigma_{\theta,n} + \Delta\sigma_{th}\left(\frac{2x}{t}\right) \\ \sigma_{z,n+1}^{Trial} = \sigma_{z,n} + \Delta\sigma_{th}\left(\frac{2x}{t}\right) \end{cases} \tag{36}$$

For the sake of simplicity and the generalization of the analysis, the parameters are normalized in the numerical solution as:

$$s_z = \frac{\sigma_z}{\sigma_y}, \quad s_\theta = \frac{\sigma_\theta}{\sigma_y}, \quad X_z = \frac{x_z}{\sigma_y}, \quad X_\theta = \frac{x_\theta}{\sigma_y}, \quad \varepsilon_z = \frac{\varepsilon_z}{\varepsilon_y}, \quad \varepsilon_\theta = \frac{\varepsilon_\theta}{\varepsilon_y}, \quad \eta = \frac{x}{t} \qquad (37)$$

The first step in the numerical procedure consists of dividing the cylinder wall thickness into n layers. Then, the increment of loads is applied with the elastic assumption. In a third step, the maximum equivalent stress in every radius is determined. Distribution of the maximum equivalent stress determines the plastic regions:

$$f(\sigma_{n+1}^{Trial}, \mathbf{x}_n) = \begin{cases} \leq 0 \Rightarrow \text{Elastic state} \\ > 0 \Rightarrow \text{Plastic flow} \end{cases} \qquad (38)$$

The solution of the Eq. (35) for plastic regions, determined in the third step, allows the plastic multiplier to be determined in every layer. The value of each parameter is updated using Eqs. (26-34). The algorithm is repeated for every layer and the stresses are recalculated by equations (12, 13). The above procedure is repeated until numerical convergence is achieved. The flowchart is given in Fig. 3.
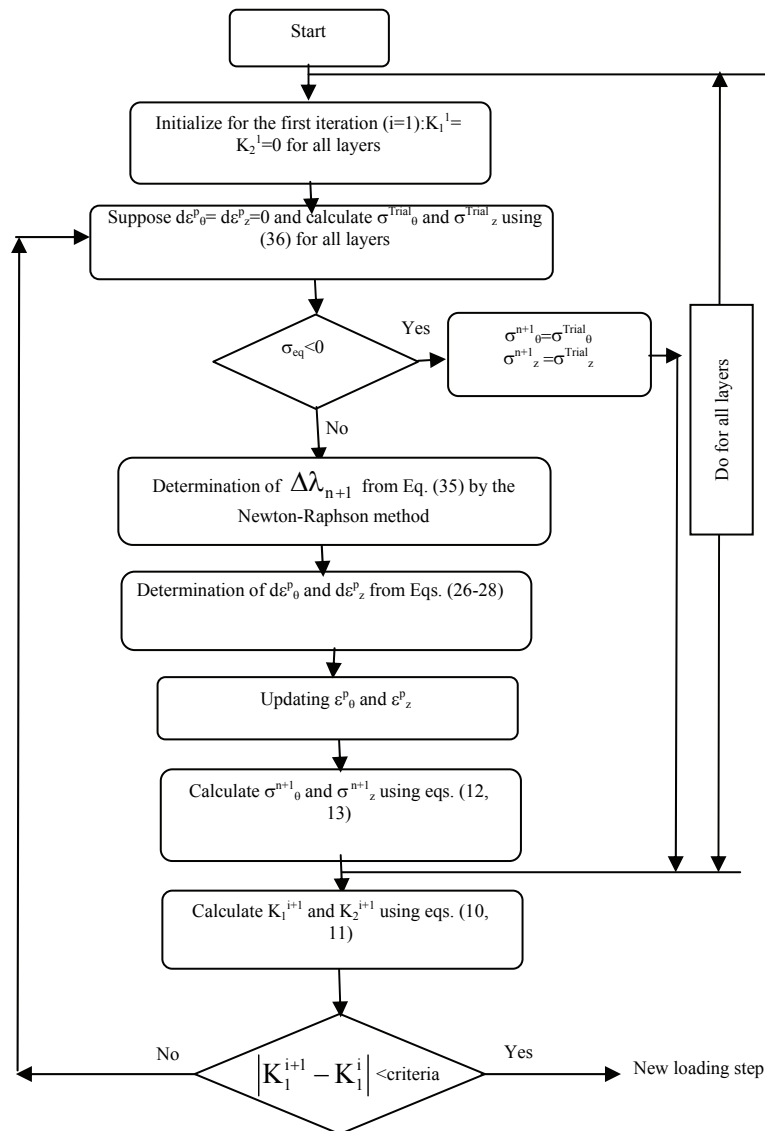


Fig. 3. Flow chart of the numerical procedure

## 5. RESULTS AND DISCUSSIONS

### a) Material and geometry specifications

Nonlinear kinematic hardening model proposed by Armstrong and Frederick was used to model the material behavior. The constants of the A-F model, the yield stress, the Young's modulus and the expansion coefficient, $\alpha$, are given in Table 1. Model constants are temperature dependent, but the average values were chosen and it was considered that the mean temperature is constant during loading and unloading. The radius and thickness are, respectively, 100 mm and 10 mm.

Table 1. Material specifications

| $\alpha$ ($10^{-6}$) /°C | C (MPa) | $\gamma$ | E (GPa) | $\sigma y$ (MPa) |
|---|---|---|---|---|
| 11 | 10 | 160 | 190 | 30 |

### b) Results and discussion

The behavior of a thin closed cylinder was investigated. Constant mechanical and cyclic thermal loading were applied. Maximum inside pressure (mechanical loading) did not exceed the yield pressure. So, the incremental loading consists of linearly increasing temperature difference distribution across the wall-thickness from zero. When the linear temperature gradient attains its maximum, it is decreased incrementally, until a zero gradient is reached. At this point a full thermal stress cycle is completed. Since each increment of the temperature gradient is less than 1°C, the number of loading increments varies in different load cases in the test matrix. Up to 100 load increments per cycle and up to 1000 cycles are applied in the most severe temperature gradients. In some cases, a steady cyclic state stress-strain answer is attained after the first cycle.

Different cylinder response is obtained in the inner and outer surface of the thin cylinder as a function of the applied mechanical and thermal loadings. In order to obtain the different regions in the Bree's diagram, more than 100 combinations of loadings were simulated. The Bree's diagram is divided into the different regions as a function of the first yield situation and the inner and outer radius behaviors. These regions are shown in Fig. 4 and explained in Table 2. Figure 4 is known as the Bree's diagram. The inner pressure and the temperature gradient are normalized as shown in equations (12, 13).

Region A corresponds to the elastic response. We increase the temperature difference and the outer surface yields. Its behavior is elastic shakedown (region B). The inner surface remains elastic. In the third part (region C), the inner surface also yields and both surfaces are in elastic shakedown. When the maximum thermal stress reaches $2\sigma_y$, the plastic strain loops are formed and plastic shakedown is obtained for the inner surface. However, the outer surface is still in elastic shakedown behavior (region D). For the thermal and mechanical stresses in the region E, the inner and outer surface has the same response and they are in a plastic shakedown state. Plastic shakedown is obtained in the axial and ratcheting in the tangential directions in the F region. Finally, ratcheting is obtained for two directions in the region G. Figures (5-7) give the stress-plastic strain and maximum plastic strain – number of cycles responses for different regions. The elastic shakedown (Fig. 5) is obtained for $\sigma_p/\sigma_y=0.7$ and $\sigma_{th}/\sigma_y=2$. The plastic shakedown behavior is shown in Fig. 6 with $\sigma_p/\sigma_y=0.1$ and $\sigma_{th}/\sigma_y=2.56$ and the ratcheting response is obtained by changing $\sigma_p/\sigma_y=0.3$ and $\sigma_{th}/\sigma_y=5.12$. Elastic and plastic shakedown was obtained after a few cycles.

Table 2. Stress regimes for Bree's cylinder behavior

| Region | Inner surface | | Outer surface | |
|---|---|---|---|---|
| | Hoop direction | Axial direction | Hoop direction | Axial direction |
| A (E) | Elastic | Elastic | Elastic | Elastic |
| B (S1) | Elastic | Elastic | Elastic Shakedown | Elastic Shakedown |
| C (S2) | Elastic Shakedown | Elastic Shakedown | Elastic Shakedown | Elastic Shakedown |
| D (S3) | Plastic Shakedown | Plastic Shakedown | Elastic Shakedown | Elastic Shakedown |
| E (PS) | Plastic Shakedown | Plastic Shakedown | Plastic Shakedown | Plastic Shakedown |
| F (R1) | Ratcheting | Plastic Shakedown | Ratcheting | Plastic Shakedown |
| G (R2&R3) | Ratcheting | Ratcheting | Ratcheting | Ratcheting |
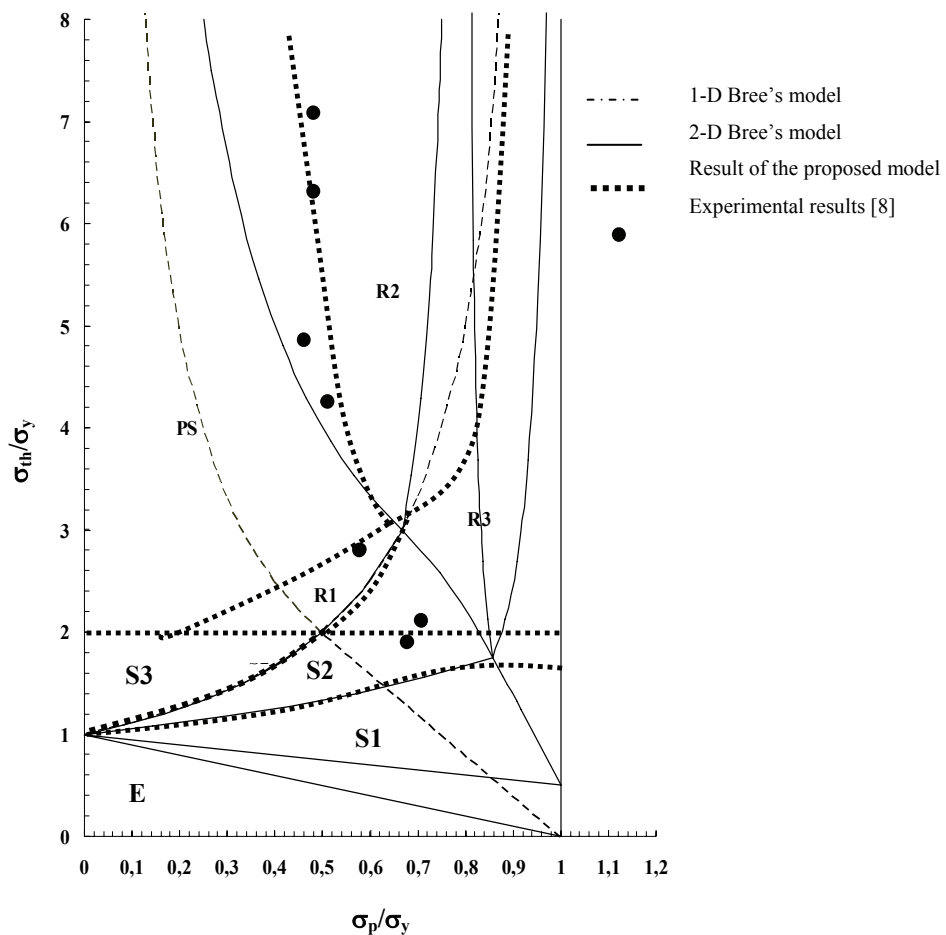


Fig. 4. Bree's diagram for a thin cylinder subjected to a constant internal
pressure and a cyclic thermal gradient

Three different ratcheting behaviors are obtained. In the R1 zone, ratcheting occurs in the hoop direction and the plastic strain did not grow more in the axial directions (F region). Ratcheting is obtained in both directions in the R1 and R2 regions. In the R1 zone the tangential stress does not exceed the yield stress and the axial stress is more than the yield stress, but in the R2 zone both stresses exceed the yield stress. There is no difference between these two cases for the Von - Mises criterion, but Bree used the Tresca's criteria and R1 and R2 zones are two distinct regions.

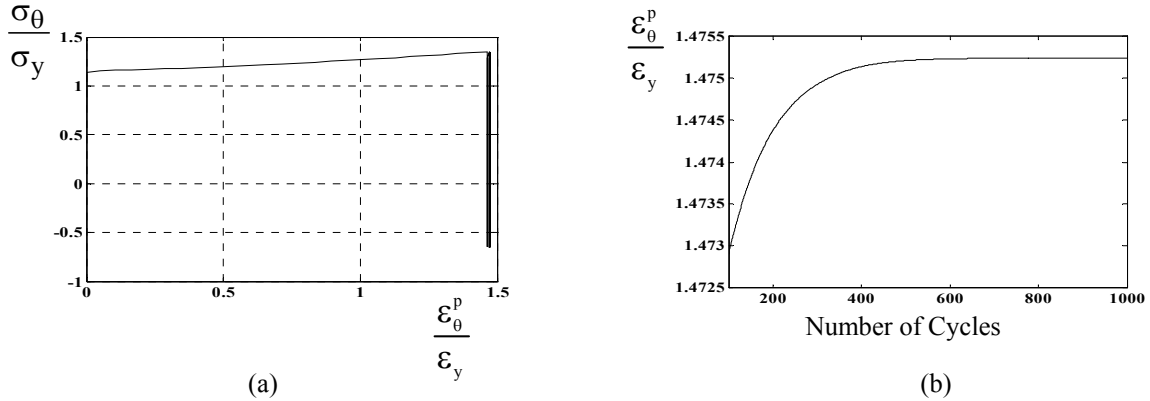(a)                                                        (b)

Fig. 5. a) Outer normalized stress – plastic strain and b) outer normalized plastic strain – cycles
in the tangential direction for $\sigma_{th}/\sigma_y=2$ and $\sigma_P/\sigma_y=0.7$

As shown in the Bree's diagram (Fig. 4) the two models of Bree are conservative, but the $2\sigma_y$ limit of the shakedown behavior is independent of the models and the material behavior. The nonlinear kinematic hardening shifts the boundary between the different regions. These results show that the ASME design code – N47, which is based on the one dimensional Bree's model, is conservative and the limit loads can be more important. In order to verify the shakedown boundary from the numerical results, the experimental shakedown boundary points obtained by Brookfield and Morten [8] on a circular strip subjected to a constant axial tension and a cyclic change of curvature, were added to Fig. 4. The numerical results correspond well with their experimental results.
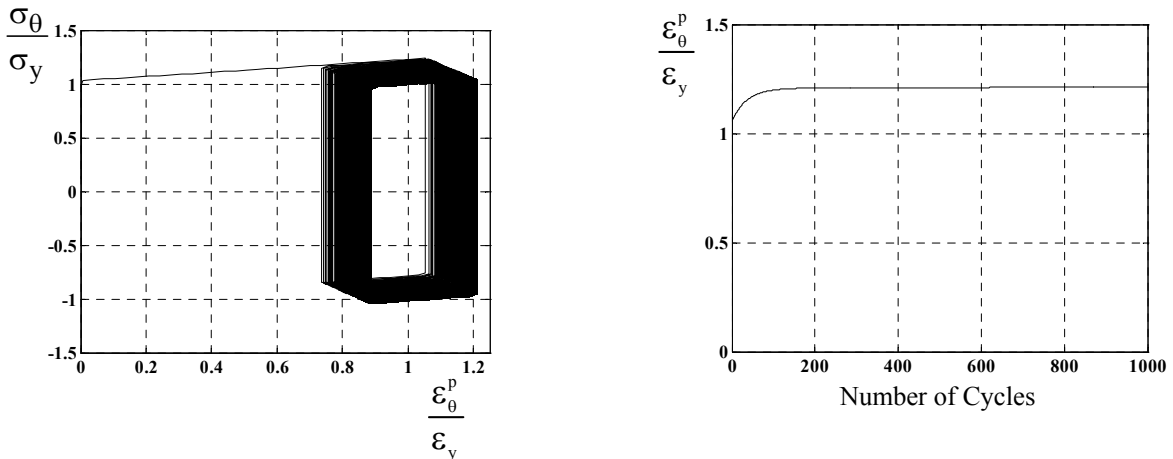


Fig. 6. a) Outer normalized stress – plastic strain and b) outer normalized plastic strain – cycles
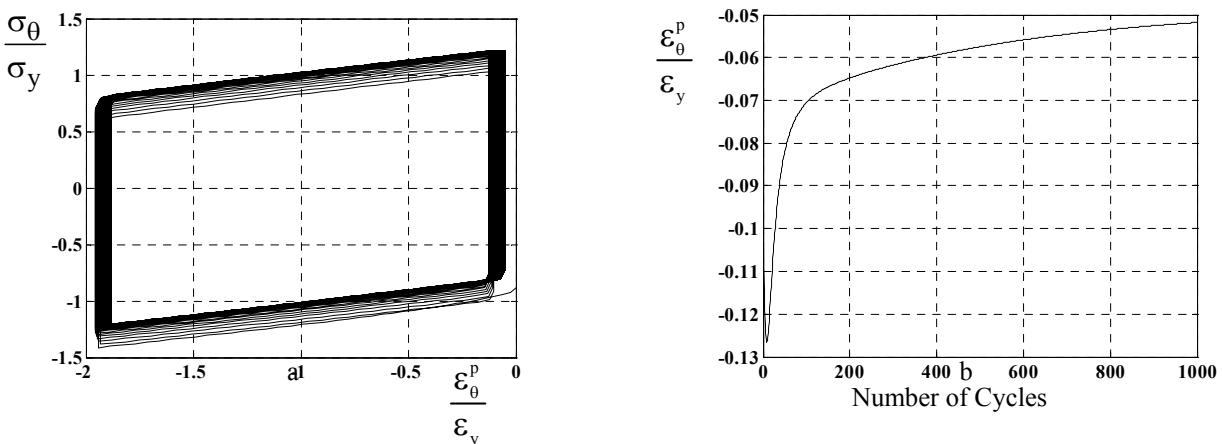in the tangential direction for $\sigma_{th}/\sigma_y=2.56$ and $\sigma_P/\sigma_y=0.1$



Fig. 7. a) Inner normalized stress – plastic strain and b) inner normalized plastic strain – cycles
in the tangential direction for $\sigma_{th}/\sigma_y=5.12$ and $\sigma_P/\sigma_y=0.3$

## 6. CONCLUSION

In this paper, the return mapping algorithm was used to obtain the answers of the Bree's tube under different combinations of the thermal and mechanical loadings. Contrary to the Bree's analysis, bi-dimensional model and the nonlinear kinematic hardening were supposed. The responses were divided into seven regions which are elastic, elastic-elastic shakedown, plastic shakedown-elastic shakedown, plastic shakedown-plastic shakedown-ratcheting-plastic shakedown and ratcheting. The supposed hardening permitted shifting of the boundaries and shows the ASME design code is conservative. The proposed iterative, which combines the return mapping algorithm and the incremental form of equilibrium and the stress-strain relations, can be used easily in the other cyclic loadings [20].

## REFERENCES

1. Bree, J. (1967). Elastic-plastic behaviour of thin tubes subjected to internal pressure and intermittent high heat fluxes with application to fast nuclear reactor fuel elements. *J. Strain Anal.* Vol. 2, pp. 226–238.

2. Bree, J. (1989). Plastic deformation of a closed tube due to interaction of pressure stresses and cyclic thermal stresses. *Int. J. of Mech. Sci.* Vol. 31, pp. 865-892.

3. Ng, H. W. & Nadarajah, C. (1996). Biaxial ratcheting and cyclic plasticity for Bree type loading-part 1: finite element analysis. *ASME J. Pressure Vessel Tech.* Vol. 118, pp. 154–60.

4. Ng, H. W. & Nadarajah, C. (1996). Biaxial ratcheting and cyclic plasticity for Bree type loading-part 2: Comparison between finite element analysis and theory. *ASME J Pressure Vessel Tech.* Vol. 118, pp 161-166.

5. Megahed, M. M., Hayhurst, D. R. & Leckie, F. A. (1982). Cyclic plastic behaviour of structural components. *Int. J. Mech. Engng.* Vol. 10, pp. 235-257.

6. Ng, H. W., Brookfield, D. J. & Moreton, D. N. (1984). A technique for conducting shakedown tests at elevated temperatures. *J. of Strain Anal.*, Vol. 20, pp.7-14.

7. Brookfield, D. J. & Moroton, D. N. (1985). The behaviour of stainless steel type 316 under Bree type loading at elevated temperatures. *8th Int. SMiRT,* Brussels, Belgium, L7/6, pp. L359-364.

8. Brookfield, D. J. & Morten, D. N. (1989) The use of a Bree simulation to investigate strain accumulation in 316 stainless steel at temperatures between room temperature and 500°C. *J. of Strain Anal.*, Vol. 24, pp. 95-102.

9. ASME Boiler and Pressure Vessel Code. (2003) Section III Division I Subsection NH, Appendix T, New York.

10. Govindarajan, S. & Sundararajan, V. (1982). Elasto-plastic behaviour of a thin cylinder thermal stress cycling. *Nuclear Eng. Des.*, Vol. 75, pp. 87-98.

11. Mahbadi, H. & Eslami, M. R. (2006). Cyclic loading of thick vessels based on the Prager and Armstrong–Frederick kinematic hardening models. *Int. J. of Pressure Vessel and Piping*, Vol. 83, pp. 409-419.

12. Armstrong, P. J. & Frederick, C. O. (1966). A Mathematical Representation of the Multi-axial Bauschinger Effect. G.E.G.B. Report RD/B/N 731.

13. Chaboche, J. L. (2008). A review of some plasticity and viscoplasticity constitutive theories. *Int. J. of Plasticity*, Vol. 24, pp. 1642-1693.

14. Marquis, D. (1979). Sur un Modèle de plasticité rendant compte du comportement cyclique. *3EME Congres Français de Mécanique*, Nancy.

15. Marquis, D. (1979). Etude théorique et vérification expérimentale d'un modèle de plasticité cyclique. *Thèse Paris VI.*

16. Karami, G. & Hematiyan, M. R. (1997). Field boundary element formulation of materially nonlinear and large deformation analysis. *Iranian J. of Science and Tech*nology, Transaction B: Engineering, Vol. 21, No. B3, pp. 229-255.

17. Wilkins, M. L. (1964) *Calculation of elastic–plastic flow.* Methods of Computational Physics, vol. 3, Academic Press, New York.

*A. Nayebi*

18. Kumar, P. & Nukala, V. V. (2006). A return mapping algorithm for cyclic viscoplastic constitutive models. *Comput. Meth. Appl. Engrg.*, Vol. 195, pp. 148-178.

19. Hopperstad, O. S. & Remseth, S. (1995). A return mapping algorithm for a class of cyclic plasticity models. *Int. J. of Num. Meth. Engrg.*, Vol. 38, pp. 549-564.

20. Nayebi, A. & El Abdi, R. (2008) Shakedown analysis of beams using nonlinear kinematic hardening materials coupled with continuum damage mechanics. *Int. J. of Mech. Sci.*, Vol. 50, pp. 1247 – 1254.